The Application of Computational Fluid Dynamics to the Study of Three-Dimensional Dynamic Stall

A. Spentzos,* G. Barakos,† K. Badcock,‡ and B. Richards§
University of Glasgow, Glasgow, Scotland G12 8QQ, United Kingdom

Abstarct
Computational fluid dynamics has been used for numerical simulations of dynamic stall in three dimensions. For multiblock structured grids, the entire Navier-Stokes equations have been solved in a time-accurate manner, together with a two-equation turbulence model when relevant. Wings with a square planform and a NACA 0012 section have been studied and found to be effective. It has been worked on to represent the flow accurately close to the wing tips, which were pointed and lacked end covers in this instance. The findings showed how the dynamic stall vortex, which in this example spans the wing like an omega with a capital

Introduction

UNLIKE fixed-wing aerodynamic design, which usually involves significant computational fluid dynamics (CFD), rotary-wing design utilizes only a small fraction of the potential that CFD has to offer. The main reason for this is the nature of the flow near the lifting surfaces, which is complex, unsteady, and turbulent. The numerical modeling of such flows encounters three main problems due to 1) the lack of robust and realistic turbulence models for unsteady separated flows, 2) the CPU time required for computing the temporal evolution, and 3) the lack of experimental data suitable for validation of the computations. This paper presents a fundamental study of the three-dimensional dynamic stall of a fi- nite wing that contains some of the important features encountered
for helicopter rotors and aircraft during maneuvers.

Dynamic stall (DS) is known to the aerodynamics community and is one of the most interesting phenomena in unsteady aero- dynamics. DS occurs when a lifting surface is rapidly pitched be- yond its static stall angle, resulting in an initial lift augmentation and its subsequent loss in a highly nonlinear manner. It has also been established that a predominant feature of DS is the presence of large vortical structures on the suction side of the lifting sur- face. These structures distort the pressure distribution and produce transient forces that are fundamentally different from their static counterparts.[1] For as long as the vortices are resident above the lift- ing surface, high values of lift are experienced that can be exploited for the design of highly maneuverable aircraft. The penalty, how- ever, is that this primary vortex eventually detaches from the surface and is shed downstream, producing a sudden loss of lift and a con- sequent abrupt change in pitching moment.[1–3] The phenomenon continues either with the generation of weaker vortices if the body remains above its static angle of attack, or is terminated if the body returns to an angle sufficiently small for flow reattachment. During DS, the flowfield includes boundary-layer growth, separation, un= steadiness, shock/boundary-layer and inviscid/viscous interactions, vortex/body and vortex/vortex interactions, transition to turbulence, flow reattachment, and relaminarization.

The importance of DS in applications is also known. Helicopter rotor performance is limited by the effects of compressibility on the advancing blade and DS on the retreating blade. Effective stall control on the retreating blade of a helicopter rotor could increase the maximum flight speed by reducing rotor vibrations and power requirements. Consequently, the study and understanding of three-dimensional DS flow phenomena would assist the rotorcraft indus- try in further pushing the design limits toward faster and more efficient rotors. In a similar way, the maneuverability of fight-ers could be enhanced if the unsteady air loads generated by DS were utilized in a controlled manner. Furthermore, improved un- derstanding of wind turbine blade DS could

O, changed over time. Both the pressure distribution on the wing's surface and the flow topology found here compare well to experimental data. The connection between the dynamic stall vortex in three dimensions and the tip vortex is crucial. According to the current findings, once the two vortices are produced, they seem to originate from the same location, which is situated close to the tip's leading edge. The formed vortex structure has a general - configuration. We believe this to be the first comprehensive numerical research of dynamic stall in three dimensions to be published in the scientific literature. enable more accu-rate engineering predictions and appreciably reduce the cost of wind energy.

Several experimental and numerical investigations for two-dimensional DS have been conducted and reported in the literature; however, much fewer have been performed for three-dimensional cases, which are the focus of this work. Regarding past work on DS, the reader is referred to the reviews by McCroskey et al.,[1] Ekaterinaris and Platzer,[4] and Carr.[2] Conclusions drawn from two- dimensional numerical investigations regarding the capabilities of CFD codes in predicting DS[4–6] can be used as a guide for three- dimensional computations. However, validation of CFD methods in three dimensions is necessary and, as will be pointed out in the next paragraphs, is a very difficult task due to the lack of adequate experimental data.

I. Previous Experimental and Numerical Work on Three-Dimensional DS

A. Experimental Investigations of Three-Dimensional DS

Three-dimensional experiments have been undertaken by Piziali,[7] Schreck and Helin,[8] Tang and Dowell,[9] Coton and Galbraith,[10] and the Aerodynamics Laboratory of Marseilles as reported in the re- cent work of Berton et al.[11,12] All of the preceding works included attempts to perform parametric investigations of the Reynolds num- ber and reduced frequency on the DS of NACA 0012 and NACA 0015 wings. Flat or rounded wing tips were used, with most of the researchers opting for measurements on half-span models equipped with splitter plates on the wing root. The experiments included har- monically oscillating and ramping motions. Quasi-steady measure- ments were also taken as part of all of the aforementioned experi- mental programs. Note that all experiments for three-dimensional DS identified in this work were conducted at low Mach num-bers. Much less work has been reported for DS at higher speeds,[3] and all works reported in the literature concern two-dimensional cases.

Piziali[7] used a NACA 0015 finite wing of aspect ratio AR 10 and conducted experiments at various reduced pitch rates and an- gles of attack for a Reynolds number of 10^6. A series of pressure transducers placed on the surface of the wing at various spanwise locations provided a comprehensive list of unsteady aerodynamic load measurements.

Tang and Dowell,[9] used a NACA 0012 square wing oscillating in pitch and took measurements along three spanwise locations for various reduced pitch rates and angles of attack. The aspect ratio of their model was 1.5. Experiments were conducted below and above the static stall angle of the wing and used to identify the onset and evolution of the dynamic stall vortex (DSV).

Schreck and Helin[8] used a NACA 0015 profile on a wing of aspect ratio 4. The Reynolds number was 6.9×10^4, and pressure transduc-

ers were placed in 11 different spanwise locations. A ramping wing motion was employed for a variety of reduced ramp rates. They also carried out dye flow visualizations in a water tunnel, in addition to providing detailed surface pressure measurements. Freymuth[13] was the first to provide a visual representation of the DSV using titanium tetrachloride flow visualization in a wind tunnel and called the observed vortical structure the omega vortex due to its shape.

Coton and Galbraith[10] and Moir and Coton[14] used a NACA 0015 square wing of aspect ratio 3 in ramp-up, ramp-down and harmonic oscillation in pitch. A relatively high Reynolds number of 1.5×10^6 was used for various angles of incidence and pitch rates. The DSV has been identified to form uniformly over the wing span, but shortly after that, the strong three dimensionality of the stall vortex, in combination with the wing tip effects, caused the DSV to distort to an ▲ shape. Surface pressure measurements, as well as smoke visualization, have been conducted.

Finally, Berton et al.[11,12] employed an embedded laser Doppler velocimetry technique to provide detailed velocity measurements in-side the boundary layer during DS, and the experiment was designed to assist CFD practitioners with their efforts in turbulence modeling.

A list of the flow conditions and measured quantities in all of the aforementioned investigations is presented in Table 1.

Among the plethora of two-dimensional experimental investiga- tions reported in the literature, Wernert et al.[15] conducted laser sheet visualization (LSV) of the flow around an oscillating NACA 0012 airfoil. This was complimented by particle image velocimetry (PIV) measurements of the flowfield. The mean angle of incidence was 15 deg, the oscillation amplitude 10 deg, and the Reynolds num- ber 3.73×10^5. The wing had an aspect ratio of 2.8, and a reduced frequency of 0.15 was used. The researchers used splitter plates on both ends of the wing to approximate two-dimensional flow conditions.

Based on the preceding summary, and because this paper fo- cuses on the flow configuration for a three-dimensional DS case, the experimental work of Schreck and Helin[8] appears to

be suitable as a starting case. This is due to the high pitch rate and the low Reynolds number employed by the researchers. It is evident from two-dimensional simulations[16] that, the higher the pitch rate, the

Table 1 Validation cases for DS^a

Conditions	Measurements
Schreck and Helin[8]	
Ramping motion,	Surface pressure,
$Re = 6.9 \times 10^4$, $M = 0.03$,	Flow visualization (dye
injection) NACA 0015, and AR = 4	
Piziali[7]	
Ramping and oscillatory motion,	Surface pressure
$Re = 2.0 \times 10^6$, $M = 0.278$,	Flow visualization
(microtufts) NACA 0015, and AR = 10	
Moir and Coton[14]	
Ramping and oscillatory motions,	Smoke visualization
$Re = 1.3 \times 10^4$, $M = 0.1$,	
NACA 0015, and AR = 3	
Coton and Galbraith[10]	
Ramping and oscillatory motions,	Surface pressure
$Re = 1.5 \times 10^6$, $M = 0.1$,	
NACA 0015, and AR = 3	
Tang and Dowell[9]	
Oscillatory motion,	Surface pressure
$Re = 0.52 \times 10^6$, and $M = 0.1$	
Berton et al.[11,12]	
Oscillatory motion,	Boundary layers
$Re = 3 \times 6 \times 10^6$, $M = 0.01$–0.3,	Velocity profiles
and NACA 0012	Turbulence quantities
Wernert et al.[15]	
Oscillatory motion,	LSV and PIV
$Re = 3.73 \times 10^5$, $M = 0.1$,	
NACA 0012, and AR = 2.8	

^{a}The first five cases concentrate on three-dimensional DS, whereas the last one em-ployed PIV for the study of the two-dimensional configuration.

easier the flow prediction is at low Mach numbers. At such condi- tions, the motion of the body is the dominant effect, and turbulence has a secondary role. Schreck and Helin[8] provided detailed surface pressure measurments that can be directly compared against CFD results. Flow visualization is also provided, but this can only be used for qualitative comparisons. In the absence of a three-dimensional data set combining flowfield and surface pressure measurements, a combination of the PIV study of Wernert et al.[15] and the surface pres- sure survey experiment of Schreck and Helin[8] provides an adequate basis of comparison for the surface pressure loads on the maneu- vering lifting surface and the velocity field and flow development around it.

B.   Past CFD Work on Three-Dimensional DS

In parallel with the experimental investigations, CFD studies have so far concentrated on two-dimensional DS cases with the earli- est efforts to simulate DS performed in the 1970s by McCroskey et al.,[1] followed later by studies. Lorber and Carta[17] and Visbal.[18] A summary of DS work up to 1997 can be found in the review paper by Ekaterinaris and Platzer.[4] Initially, compressibility effects were not taken into account due to the required CPU time for such calculations. However, in the late 1990s, the problem was revisited by many researchers[5,19–21] and issues such as turbulence modeling and compressibility effects were addressed. Still, due to the lack of computing power and established CFD methods, most CFD work until now has focused on the validation of CFD codes rather than the understanding of the flow physics. Barakos and Drikakis,[5,16] Ekaterinaris and Menter,[22] and Rizetta and Visbal[23] have assessed several turbulence models in their two-dimensional studies, stress- ing their importance for the realistic representation of the flowfield encountered during DS.

The only CFD works published to date on three-dimensional DS are by Ekaterinaris[20] on the turbulent flow regime and by Newsome[24] on laminar flow. The computations by Ekaterinaris were conducted at relatively low incidence angles, and, consequently, the three- dimensional DSV was not fully formed, and the presented histories of the integral loads indicated some hysteresis and light stall of the wing instead of a DS flow. As reported,[20] the grid resolution near the wing tip was not adequate for the tip vortex to be fully resolved. The same situation arises in the work of Newsome,[24] where the employed grid did not allow for adequate modeling of the sharp wing tip. Both researchers demonstrated that three-dimensional computations are possible, provided adequate grids are employed. An additional work by Morgan and Visbal[25] also discussed the three-dimensional as- pects of DS. The objective of the researchers was the simulation of flow around a wing spanning the test section of a tunnel without any tips exposed to the freestream. However, the presence of a tip vortex can influence the evolution of the three-dimensional DSV as will be discussed in the following paragraphs. The importance of the tip vortex and the difficulties in CFD solutions for the near-tip region of wings with sharp tips are discussed in the work by Snyder and Spall[26] for steady-state flow. This investigation is important for the present work because the experiments by Schreck and Helin[8] were conducted on a model with sharp tips. This interaction between the DSV and the tip vortex has not been discussed in any of the previous CFD works on three-dimensional DS.[20,24] Interestingly, the experi- mental works by Lorber[27] and Freymuth[13] mention the importance of such interactions for square wings and even for delta-wing cases. The present work is, to our knowledge, the first systematic attempt to investigate this interaction of vortices during three-dimensional DS using CFD.

II. CFD Method and Grid Generation

The details of the employed CFD solver can be found in Ref. 28. Only a summary is given in this paper. The code is capable of solving flow conditions from inviscid to fully turbulent using the Reynolds-averaged Navier–Stokes (RANS) equations in three dimensions. Dettached-eddy simulation and large-eddy simulation options are available, though these were not used in this work. Because of the flow conditions considered here, simple two-equation turbu-lence models have been employed. Most of the results presented in this paper have been obtained using the baseline k–ω model.[29] To solve the RANS equations, multiblock grids were generated around the required geometries, and the equations were discretized us-ing the cell-centered finite volume approach. For the discretization of the convective fluxes, Osher's scheme has been used. A formally third-order accurate scheme is achieved using a MUSCL interpola-tion technique. Viscous fluxes were discretized using central differ-ences. Boundary conditions were set using two layers of halo cells. The solution was marched in time using an implicit second-order scheme, and the final system of algebraic equations was solved using a preconditioned Krylov subspace method.

Meshing finite wings encounters a problem in the tip region be-cause a single-block grid will 1) render flat tips topologically im-possible and 2) lead to skewed cells in the case of rounded tips. To counter these problems, three different blocking strategies were adopted as shown in Fig. 1. In a first attempt, shown in Fig. 1a, the tip end is formed by a two-dimensional array of collapsed cells result-ing in a C–H single-block topology. Although this is adequate for thin, sharp tips, it fails to represent satisfactoraly the tip geometry of wings with thicker sections or flat tips. For wings with flat tips, such as the ones studied in this paper, good results can be obtained by using a true multiblock topology. As shown in Fig. 1b, the tip plane constitutes one of the six sides of a new block extending to the farfield. This topology can generate both flat and rounded tips and produces no collapsed cells in the vicinity of the tip region. A modification of this topology is shown in Fig. 1c, where four blocks were used next to the flat tip plane to promote cells with a better aspect ratio than in the preceding case. Other approaches in-cluding H–H and C–O topologies have also been investigated. The latter is shown in Fig. 1d and is suitable for truncated wings with rounded tips. In this case, the C topology used around the leading-edge curves around the tip resulted in a very smooth distribution of the radial mesh lines around the entire wing and, in particular, at the wing–tip interface, which is no longer treated as a block boundary. This blocking produces the smoothest mesh around the tip region because none of the emerging grid cells is skewed. Apart from the single-block C–H method, all other topologies can be used for both rounded and flat wing tips. The details of all grids used in this study are listed in Table 2.

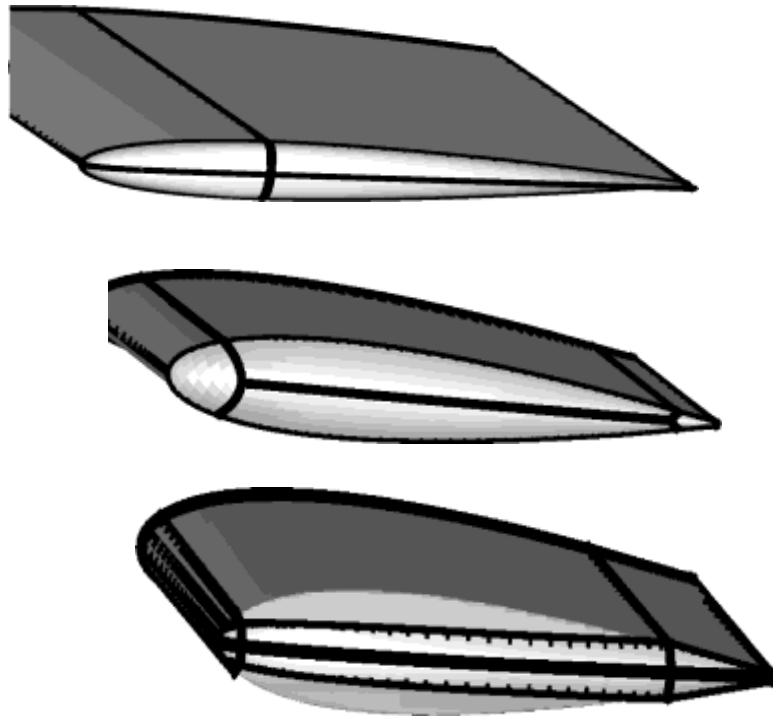**Fig. 1 Grid topologies employed for calculations: a) collapsed tip and b, c, and d) extruded tips.**

Table 2 Details of employed CFD grids and time required for calculations[a]

Grid	Blocks	Points on wing	Points on tip	Size, nodes	Wall distance	Grid topology	CPU time, h	Number of CPUs
1	13	6,222	820	420,000	$10^{-4}c$	Fig. 1b	255	1
2	20	7,100	900	729,000	$10^{-4}c$	Fig. 1c	31.1	8
3	44	8,400	900	1,728,000	$10^{-4}c$	Fig. 1c	111.1	8
4	64	18,900	4,500	2,727,000	$10^{-5}c$	Fig. 1c	100	24
5	6	240	n/a	62,400	$10^{-5}c$	Two-dimensional C type	17.5	1
6	6	360	n/a	108,000	$10^{-5}c$	Two-dimensional C type	38.9	5

[a]For all cases the far-field boundary of the computational domain was located at 10 chord lengths away from wing surface; all calculations were performed on a Linux Beowulf cluster with 2.5-GHz Pentium-4 nodes.
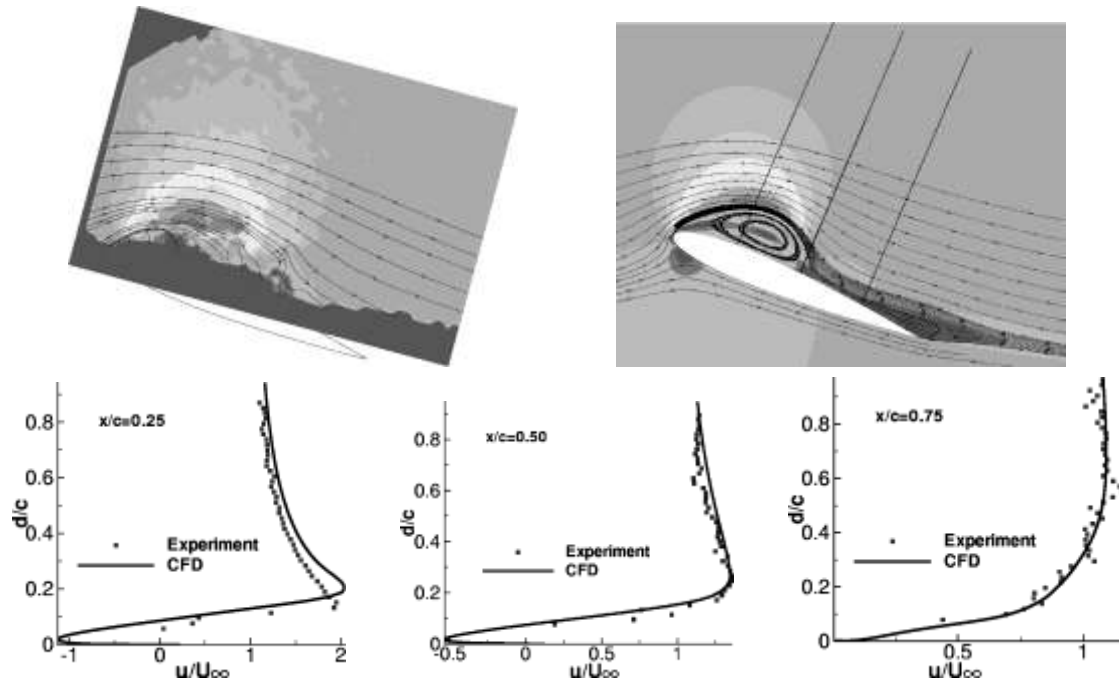
a) Angle of attack = 22 deg upstroke
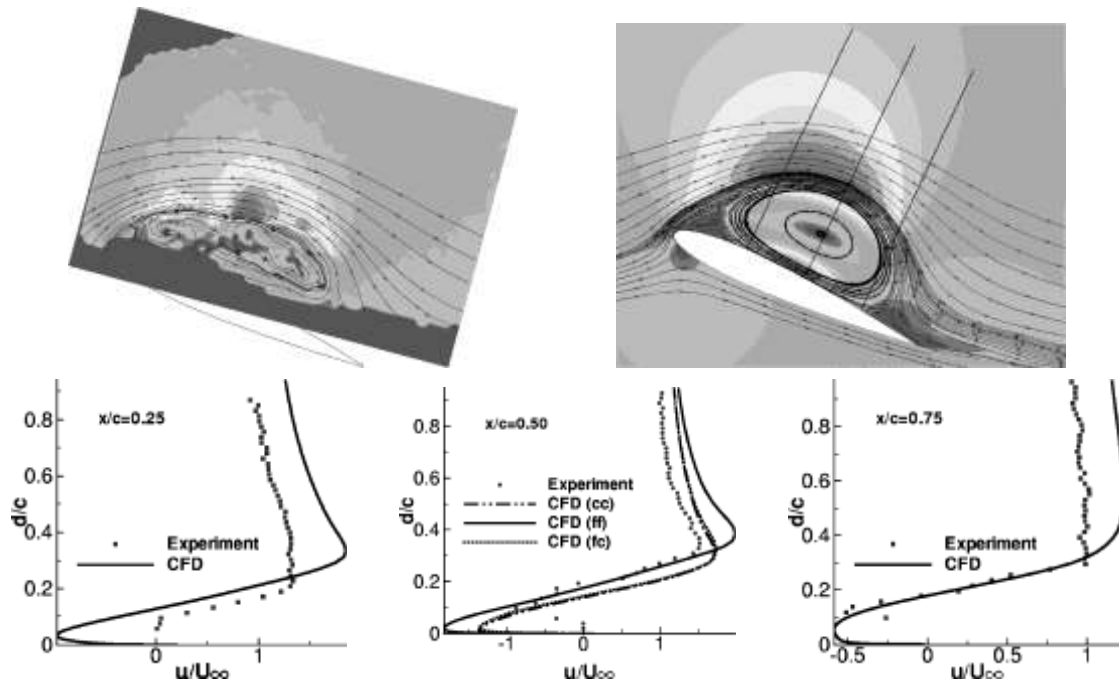
b) Angle of attack = 24 deg upstroke

Fig. 2 Comparison between CFD and experiments by Wernert et al.,[15] where streamlines have been superimposed on color maps of velocity magnitude and, for experimental cases, are based on PIV data: $\alpha(t) = 15 - 10$ deg $\cos(kt)$, $k = 0.15$, $Re = 3.73 \times 10^5$, $M = 0.1$, and $x/c_{\text{rot}} = 0.25$.

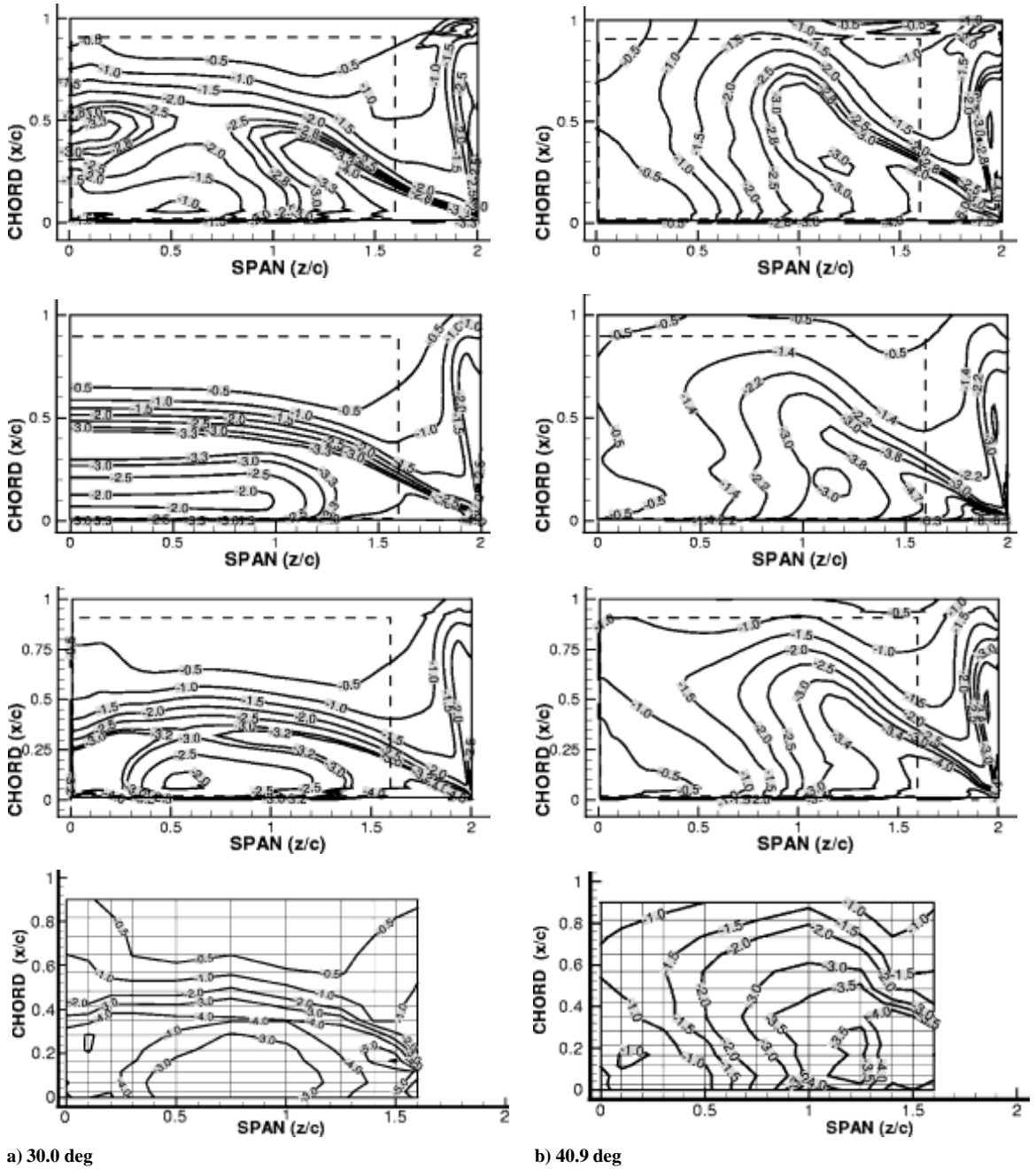a) 30.0 deg   b) 40.9 deg

Fig. 3 Comparison between experiments by Schreck and Helin[8] and CFD results for surface coefficient distribution on suction side of rectangular NACA 0015 wing, where flow conditions are $a^+ = 0.1$, $Re = 6.9{\times}10^4$, $M = 0.03$, and $x/c_{rot} = 0.33$, with ramping motion between 0 and 60 deg of incidence; from top to bottom, CFD with splitter plate as a viscous wall and laminar conditions, CFD with splitter plate as symmetry plane, CFD with splitter plate as viscous wall, and experimental values.

III. Results and Discussion

A. Prediction of the Flowfield Around Oscillating Airfoil

The first target of the present work is to compute the two-dimensional velocity field during dynamic stall and compare against tunnel measurements. This is essential because in the following paragraphs the flow configuration during three-dimensional DS is to be analyzed, and confidence must be established on the accuracy of the emplyed CFD method. Although every effort was made to find velocity field measurements for CFD validation in the litera- ture, the case by Wernert et al.[15] was the only finding. In Fig. 2, the flowfield measurements of Wernert et al.[15] are compared with the present CFD results. Two angles of attack were selected dur- ing the oscillation cycle. The CFD calculations were made at the same conditions as the experiment, with a sinusoidal pitch of the form $\alpha(t) = 15 - 10$ deg $\cos(kt)$ at a reduced pitch rate of $k = 0.15$, $Re = 3.73 \times 10^5$, and $M = 0.1$. The comparison between CFD and experiments is remarkably good, with the DSV predicted at

almost the same position as in the measurements. The evolution of DS is similar to that described by previous authors.[16] A trailing-edge vor- tex appears at high incidence angles, and below the DSV, a system of two secondary vortices is formed. Despite the lack of measurements of the surface pressure, the PIV study of Wernert et al.[15] provides the rare opportunity for comparing the computed velocity field against quantitative measurements. In this work, velocity profiles were ex-tracted at three chordwise stations corresponding to x/c 0.25, 0.5, and 0.75. With the exception of the work reported by Barakos and Drikakis in Ref. 30, this is the only other comparison of velocity profiles during DS appearing in the literature. As shown in Fig. 2, the comparison between experiments and CFD is remarkably good at the lowest incidence angle (Fig. 2a) and remains favorable even at higher incidence angle (Fig. 2b). Wernert[15] reported that, at the angles of 23 and 24 deg, the flowfield was no longer reproducible

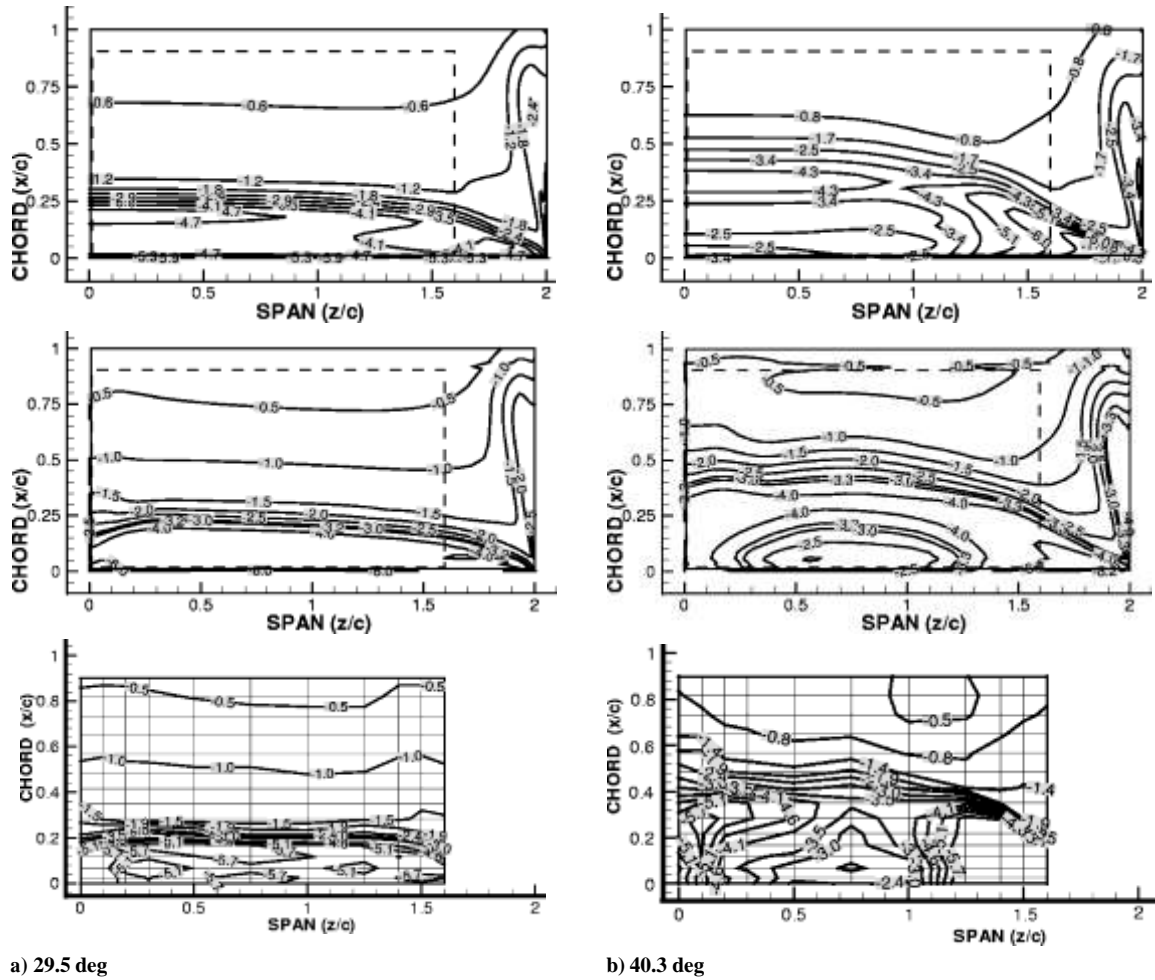a) 29.5 deg   b) 40.3 deg

Fig. 4 Comparison between experiments by Schreck and Helin[8] and CFD results for surface coefficient distribution on suction side of rectangular NACA 0015 wing; from top to bottom: CFD with splitter plate as symmetry plane, CFD with splitter plate as viscous wall, and experimental values $a^+ = 0.2$, $Re = 6.9 \times 10^4$, $M = 0.03$, and $x/c_{rot} = 0.25$, with ramping motion between 0 and 60 deg of incidence.

during the experiments, which explains the discepancies observed. The agreement is better closer to the wall, whereas a constant shift appears toward the outer part of the boundary layer. The shape of the profile is, however, well predicted. Further comparisons of the turbulent flow quantities in this unsteady flow are not possible due to the lack of near-wall resolution of the PIV measurements. Note from Fig. 2b that the effect of the spatial and temporal results is strong. Figure 2b shows three plots corresponding to the coarse grid with coarse time, fine grid with fine time, and fine grid with coarse time. The details of the grids are given in Table 2. Grids 5 and 6 were used for the prescribed cases, and the final results were obtained on

grid 6. The coarse time discretization corresponds to 80 time steps per cycle, whereas the fine time discretization corresponds to 200 time steps per cycle. The resolution even of the coarse time step corresponds to three unsteady calculations per degree of incidence.

### B. Three-Dimensional DS Cases: Validation of Method

A second set of calculations simulated the experiment of Schreck and Helin.[8] This is a good validation case because the experiment was conducted at low Reynolds numbers and turbulence model- ing issues are secondary. In addition, the employed ramping rates were high so that the flow is mainly

driven by the forced motion of the body. At slower ramping rates, it is expected that the influence of turbulence, transition, and viscous effects will be stronger. For this work, both laminar and turbulent flow calculations have been performed. Note that the flow conditions of Newsome's study[24] are close to, but not the same as, the ones used here. This is be- cause Newsome's calculations were compared against water-tunnel visualization (at $Re = 5.6 \times 10^4$) and pressure data from Ref. 31,

whereas the current set of experimental data comes from wind-tunnel experiments[8] at Re 6.9 10^4. In contrast to the previous laminar flow study by Newsome,[24] where rounded tips were used instead of sharp ones, the present work preserves the real geometry of the wing using multiblock grids as explained in the preceding sections. This was found to be necessary because there is a strong interaction between the tip and the DS vortices. Three CFD grids were constructed: The coarse grid has 0.7 million cells, the medium has 1.7 million cells, and the fine has 2.7 million cells. The medium grid was found to be adequate following comparisons of the integral loads of the wing between the three grids and was employed for the rest of the calculations. Even results on the coarse grid were

found to be close to those obtained on finer meshes for incidence angles below stall. It has to be noted that although experiments were con- ducted at a Mach number of 0.03, CFD results were obtained at 0.2. A time-step sensitivity study was subsequently conducted by halving the original time step. The results of the two calculations were practically the same, and, therefore, the original time step was considered adequate. This dimensionless time step of 0.058 corre- sponds to a real time step of 10^{-3} s and results in four unsteady flow solutions per degree of incidence. The required CPU time for calculating the two-dimensional and three-dimensional flow cases is reported in Table 2. All calculations were performed on a Beowulf cluster with 2.5-GHz Pentium-4 nodes.

Comparisons against measurements are presented in Fig. 3 where C_p contours on the upper surface of the wing are plotted. Measure- ments are only available on part of the wing area,[8] bounded by a dashed box on the CFD plots. Three sets of calculations are shown, including laminar flow results with the inboard boundary plane of the computational domain assigned a viscous wall boundary condition,

$z/c = 1.0$ and $a^+ = 0.1$

$z/c = 1.6$ and $a^+ = 0.1$

$z/c = 1.0$ and $a^+ = 0.2$
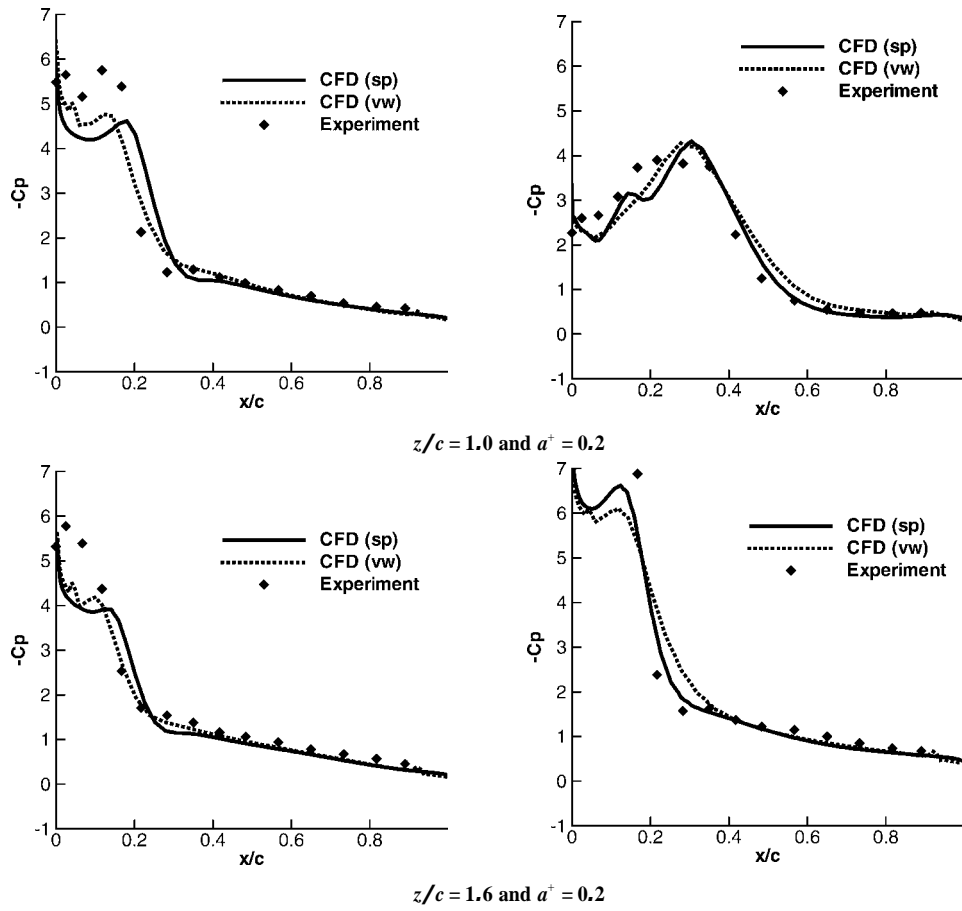

$z/c = 1.6$ and $a^+ = 0.2$
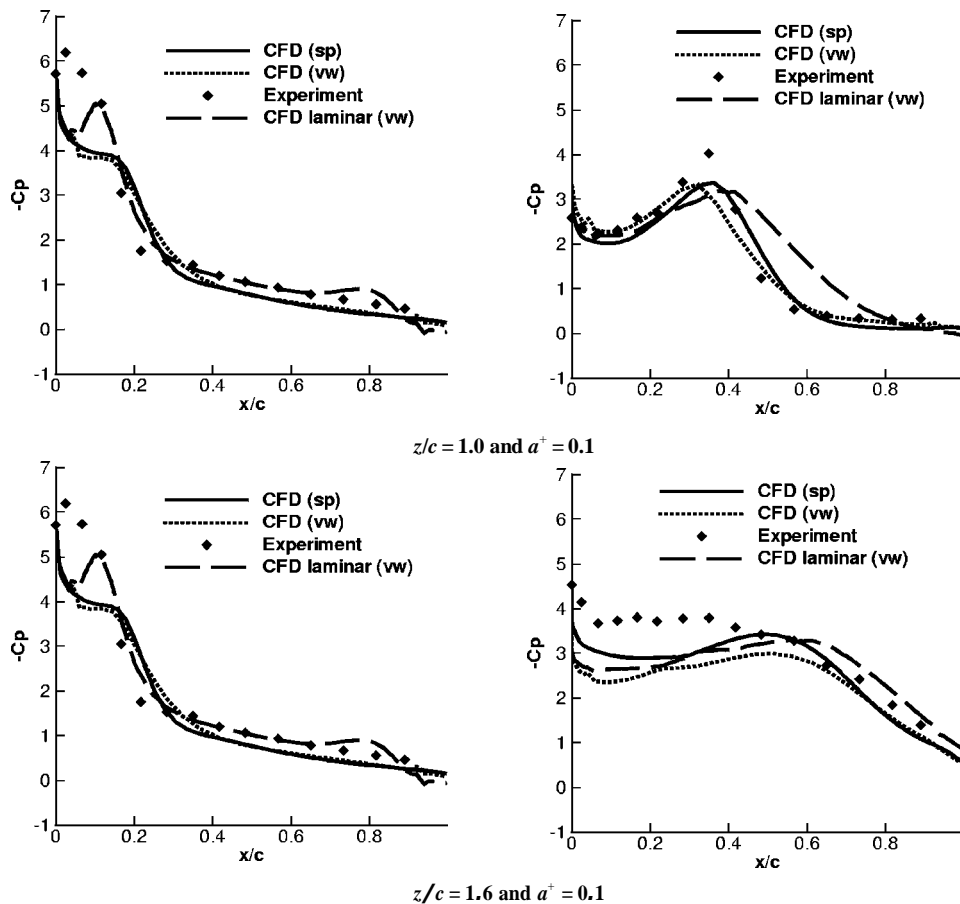
Fig. 5 Comparison between experiments and simulation for surface pressure coefficient distribution at incidence angles of 30 deg (left) and 40 deg (right); both cases with splitter plate as symmetry plane and splitter plate as viscous wall: $Re = 6.9 \times 10^4$, $M = 0.2$, and $x/c_{rot} = 0.25$, with ramping motion between 0 and 60 deg of incidence.
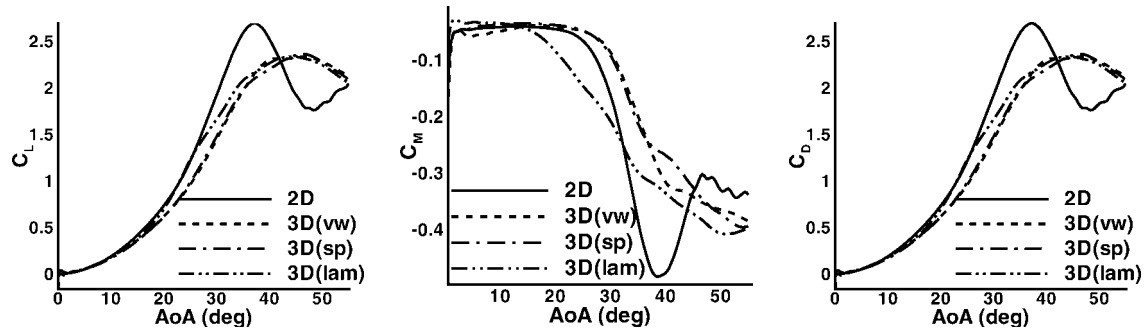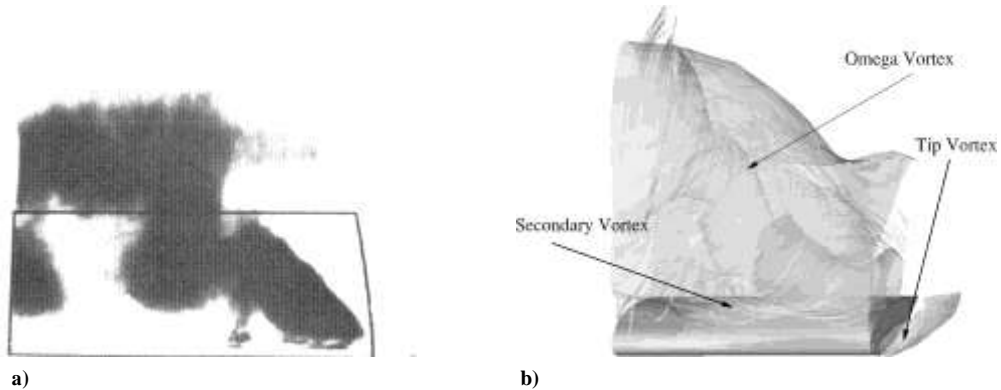

Fig. 6 Comparison between two-dimensional and three-dimensional simulation results for lift, drag, and quarter-chord moment coefficient: $a^+ = 0.1$, $Re = 6.9 \times 10^4$, $M = 0.2$, and $x/c_{rot} = 0.25$, with ramping motion between 0 and 60 deg of incidence.
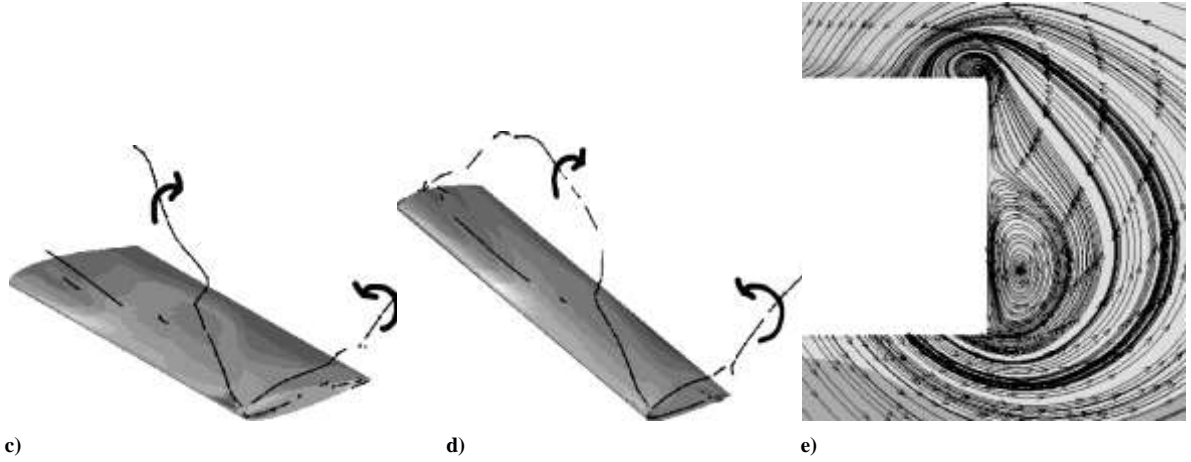

a)

b)

c)   d)   e)

**Fig. 7 Flow topology during three-dimensional DS: a) the Ω-shaped vortex as shown from the visualizations performed by Schreck and Helin,[5]
b) CFD results, c) vortex cores from CFD with symmetry condition at the midspan plane, d) vortex cores from CFD with a viscous wall condition at
the midspan plane, and e) tip vortex formation at the quarter-chord plane normal to the wing.**

turbulent flow results with symmetry plane condition, and turbu-lent flow results with viscous wall condition. The same number of contours and at the same levels were drawn for experiments and CFD. The concentration of the contour lines near the midchord cor-responds to the location of the DSV. One can clearly see that at 30 deg of incidence that the simulation results with a viscous wall condition are in much better agreement with the experiments. It is difficult to decide which of the laminar and turbulent flow results are in better agreement with experiments; however, toward the tip region of the wing the simulation with the turbulence model pro-vides a better comparison, predicting more accurately the location of the DSV. Overall, the shape and level of the contours corresponds to the measured data with the agreement getting better at higher incidence angles. The reason for any minor discrepancies toward the midspan of the wing lies in the fact that the experiment used a splitter plate on the wing root with surface qualities that do not exactly match the idealizations made by either symmetry or viscous boundary conditions. The size of the plate is comparable with the DSV size (splitter plate diameter being equal to two chord lengths), and, thus, the effectiveness of the plate may not be good, espe-cially at high incidence angles. Because of the size of the splitter plate, results with viscous wall condition at midspan are closer to the experiments for low incidence; however, symmetry plane re-sults tend to be better at higher angles. This is because the DSV moves away from the surface of the wing and expands beyond the splitter plate.

C. Three-Dimensional DS: Analysis of Flowfield

With established confidence on the grid and time steps used, fur-ther computations were attempted. Figures 7a and 7b present a com-parison between experiments[8] and CFD flow visualization for the fully formed ▲-shaped vortex. The agreement in the overall shape is clear. The DS vortex is completely detached from the wing inboard and bends toward the surface of the wing outboard. An additional feature of the flow (not evident from the experimental flow visualiza-tion) is the presence of the secondary vortices below the ▲-shaped vortex. Furthermore, the tip and the ▲-shaped vortices approach the same point near the tip.

Figures 7c and 7d present the configuration of the Π–▲ vortex system for the cases of symmetry midspan conditions (Fig. 7a) and a viscous wall (Fig. 7b). Note that the viscous wall has the effect of bending the ▲ vortex toward the junction of the wing and the plate, giving it a very high curvature. The symmetry condition has a smaller effect and approximates the two-dimensional condition better; the DSV quickly dettaches from the wing and is convected downstream. It appears that the leading edge of the tip is a singularity point where the Π–▲ system stays attached on the solid surface. At this point, the freestream

can feed both vortices with momentum. In terms of Helmholtz's vortex theorems, this flow configuration is very interesting. The DSV cannot end up in the freestream but is forced to either join the tip vortex or end on a solid surface. This is further assisted by the sharp tip of this particular wing. As reported in Ref. 26 and verified in this work (Fig. 7e), at incidence angles below stall, a system of vortices develops around the tip that eventually leads to the formation of the tip vortex. As can be seen in Fig. 7e, even at low incidence angles a vortex is present on the wing and the DSV, once created, moves toward this vortex and forms with it a vortical system.

The evolution of the DSV is largely dependent on the midspan boundary conditions. Modeling the midspan as a viscous wall in-duces a vortical structure whose center is the trace of the pitch axis (PA) onto the midspan plane, and angular velocity is the angular ve-locity of the wall. However, during the early stages of the formation of the DSV, the DSV and this viscous wall vortex are of comparable strength, and they tend to merge. The consequence of this interac-tion is the tendency of the inboard part of the DSV to appear close to the PA location. In the case of the midspan plane being modeled as a symmetry plane, no such relation seems to exist between the PA and the appearing location of the DSV. Similar remarks have been reported in Ref. 24.

For both cases of the viscous wall and symmetry plane midspan conditions, the secondary vortex that appears under the DSV and close to the leading edge of the wing merges with the DSV as the latter approaches the wing surface toward the tip.

A set of snapshots from the CFD calculations is presented in Fig. 8. In Fig. 8, the cores of the vortices are extracted from the CFD solutions using the vortex core detection toolbox in FieldView[TM] and are tracked in time. In addition, particles were used to highlight the size of the vortices and their interactions. The phenomenon starts inboard with the formation of a vortex at the leading edge, which is subsequently detached from the wing and grows in size. The growth reduces as one moves toward the tip of the wing (Fig. 8a) and the core of the vortex bends upstream toward the leading edge of the wing tip (Fig. 8b). Further on during the cycle, one cannot fail to note that on the midspan of the wing (Fig. 8c) the flow looks like the two-dimensional cases of Fig. 2. However, as the DSV is formed, the core of the vortex stays bound to the leading edge region of the wing tip, whereas the main part of the DSV is convected down-stream. As the DSV grows in size and its core moves above the surface of the wing, the ▲-shape appears because near the wing tip, the vortex is still bound. The phenomenon becomes more and more interesting as the tip vortex is formed, leading to a Π–▲ vortex con-figuration that is a combination of the two well-established vortical systems: the tip vortex that

appears for all wing tips and the DSV that is unique to unsteady flows. The flow near the leading edge of the wing tip is complex, and the streamtraces originating just up- stream of the tip are directed either toward the tip vortex or the DSV. Apart from the main vortices, all secondary vortices appearing dur-ing two-dimensional DS are present in the three-dimensional case. Interestingly, the secondary vortices formed below the DSV also appear to take the same ▲ shape and bend at the leading edge of the wing tip.

IV. Conclusions

Numerical simulation of the three-dimensional DS phenomenon has been undertaken, and results have been compared against ex- perimental data as well as two-dimensional computations. For all cases, CFD results compare favorably with experiments, given the complexity of the problem. The three-dimensional structure of the DSV and the time evolution of the DS phenomenon were revealed and found to agree well with the only flow visualization study avail- able. The main conclusion of this work is that similarity between two-dimensional and three-dimensional calculations is good only in the midspan area of the wing, whereas the outboard section is dominated by the interaction of the ▲-shaped vortex with the tip vortex. At the conditions considered here, the flow configuration near the wing tip is far more complex, with the tip vortex and the DSV merging toward the wing tip. The presence of a symmetry plane at the midspan was found to alter the shape of the ▲ vortex. From this study, it is evident that

further experimental and numerical investigations of this complex flow phenomenon are necessary. In particular, combined efforts with well-controlled experiments and measurements of both surface and boundary-layer properties are es- sential to evaluate the predictive capabilities of CFD. This work is part of a wider effort undertaken by the authors in understanding, predicting, and controlling unsteady aerodynamic flows. Based on the current results, an obvious step is to further our investigation on the effect of the Reynolds number and turbulence of the evolution of the DSV. Experimental data at higher Reynolds numbers are rare, especially when velocity measurements are needed. The cases by Berton et al. and Coton and Galbraith appear to be appropriate for validating CFD, and future efforts will start from CFD validations of these two cases.

References

[1]McCroskey, W. J., Carr, L. W., and McAlister, K. W., "Dynamic Stall Experiments on Oscillating Aerofoils," *AIAA Journal*, Vol. 14, No. 1, 1976, pp. 57–63.

[2]Carr, L. W., "Progress in Analysis and Prediction of Dynamic Stall," *Journal of Aircraft*, Vol. 25, No. 1, 1988, pp. 6–17.

[3]Carr, L. W., and Chandrasekhara, M. S., "Compressibility Effects on Dynamic Stall," *Progress in Aerospace Sciences*, Vol. 32, No. 6, 1996, pp. 523–573.

[4]Ekaterinaris, J. A., and Platzer, M. F., "Computational Prediction of Airfoil Dynamic Stall," *Progress in Aerospace Sciences*, Vol. 33, No. 11–12, 1997, pp. 759–846.

[5]Barakos, G. N., and Drikakis, D., "Unsteady Separated Flows over Ma- noeuvring Lifting Surfaces," *Philosophical Transactions of the Royal Society of London, Series A: Mathematical and Physical Sciences*, Vol. 358, 2000, pp. 3279–3291.

[6]Barakos, G. N., and Drikakis, D., "An Implicit Unfactored Method for Unsteady Turbulent Compressible Flows with Moving Boundaries," *Com-puters and Fluids*, Vol. 28, No. 8, 1999, pp. 899–922.

[7]Piziali, R. A., "2-D and 3-D Oscillating Wing Aerodynamics for a Range of Angles of Attack Including Stall," NASA TM-4632, Sept. 1994.

[8]Schreck, S. J., and Helin, H. F., "Unsteady Vortex Dynamics and Surface Pressure Topologies on a Finite Wing," *Journal of Aircraft*, Vol. 31, No. 4, 1994, pp. 899–907.

[9]Tang, D. M., and Dowell, E. H., "Experimental Investigation of Three-Dimensional Dynamic Stall Model Oscillating in Pitch," *Journal of Aircraft*, Vol. 32, No. 5, 1995, pp. 163–186.

[10]Coton, F. N., and Galbraith, R. A. M., "An Experimental Study of Dy- namic Stall on a Finite Wing," *Aeronautical Journal*, Vol. 103, No. 1023, 1999, pp. 229–236.

[11]Berton, E., Allain, C., Favier, D., and Maresca, C., "Experimental Methods for Subsonic Flow Measurements," *Progress in Computational Flow–Structure Interaction*, edited by W. Haase, V. Selmin, and B. Winzell, Notes on Numerical Fluid Mechanics and Multidisciplinary Design, Vol. 81, Springer, 2003, Chap. 2.10.

[12]Berton, E., Allain, C., Favier, D., and Maresca, C., "Database for Steady and Unsteady 2-D and 3-D Flow," *Progress in Computational Flow– Structure Interaction*, edited by W. Haase, V. Selmin, and B. Winzell, Notes on Numerical Fluid Mechanics and Multidisciplinary Design, Vol. 81, Springer, 2003, Chap. 3.2.

[13]Freymuth, P., "Three-Dimensional Vortex Systems of Finite Wings," *Journal of Aircraft*, Vol. 25, No. 10, 1988, pp. 971, 972.

[14]Moir, S., and Coton, F. N., "An Examination of the Dynamic Stalling of Two Wing Planforms," Dept. of Aerospace Engineering, Aerospace En- gineering Rept. 9526, Univ. of Glasgow, Glasgow, Scotland, U.K., 1995.

[15]Wernert, P., Geissler, W., Raffel, M., and Kompenhans, J., "Experimen- tal and Numerical Investigations of Dynamic Stall on a Pitching Airfoil," *AIAA Journal*, Vol. 34, No. 5, 1996, pp. 982–989.

[16]Barakos, G. N., and Drikakis, D., "Computational Study of Unsteady Turbulent Flows Around Oscillating and Ramping Aerofoils," *Interna- tional Journal for Numerical Methods in Fluids*, Vol. 42, No. 2, 2003, pp. 163–186.

[17]Lorber, P. F., and Carta, F. O., "Airfoil Dynamic Stall at Constant Pitch Rate and High Reynolds Number," *Journal of Aircraft*, Vol. 25, No. 6, 1988, pp. 548–556.

[18]Visbal, M. R., "Dynamic Stall of a Constant-Rate Pitching Airfoil," *Journal of Aircraft*, Vol. 27, No. 5, 1990, pp. 400–407.

[19]Patterson, M. T., and Lorber, P. F., "Computational and Experimental Studies of Compressible Dynamic Stall," *Journal of Fluids and Structures*, Vol. 4, No. 3, 1990, pp. 259–285.

[20]Ekaterinaris, J. A., "Numerical Investigation of Dynamic Stall of an Oscillating Wing," *AIAA Journal*, Vol. 33, No. 10, 1995, pp. 1803–1808.

[21]Ekaterinaris, J. A., Shrinivasan, G. R., and McCroskey, J. W., "Evalu- ation of Turbulence Models for Unsteady Flows of an Oscillating Airfoil," *Computers and Fluids*, Vol. 24, No. 7, 1995, pp. 831–861.

[22]Ekaterinaris, J. A., and Menter, F. R., "Computation of Oscillating Air- foil Flow with One- and Two-Equation Turbulence Models," *AIAA Journal*, Vol. 32, No. 12, 1994, pp. 2359–2365.

[23]Rizzetta, D. P., and Visbal, M. R., "Comparative Numerical Study of Two Turbulence Models for Airfoil Static and Dynamic Stall," *AIAA Journal*, Vol. 31, No. 4, 1993, pp. 784–786.

[24]Newsome, R. W., "Navier–Stokes Simulation of Wing–Tip and Wing–Juncture Interactions for a Pitching Wing," AIAA Paper 94-2259, June 1994.

[25]Morgan, P. E., and Visbal, M. R., "Simulation of Unsteady Three-Dimensional Separation on a Pitching Wing," AIAA Paper 2001-2709, June 2001.

[26]Snyder, D. O., and Spall, R. E., "Numerical Investigation into Multiple Vortex Structures Formed over Flat End-Cap Wings," *AIAA Journal*, Vol. 38, No. 8, 2000, pp. 1486–1488.

[27]Lorber, P. F., "Tip Vortex, Stall Vortex and Separation Observations on Pitching Three-Dimensional Wings," AIAA Paper 93-2972, July 1993.

[28]Badcock, K. J., Richards, B. E., and Woodgate, M. A., "Elements of Computational Fluid Dynamics on Block Structured Grids Using Im- plicit Solvers," *Progress in Aerospace Sciences*, Vol. 36, No. 5–6,

2000, pp. 351–392.

[29]Wilcox, D. C., "Reassessment of the Scale-Determining Equation for Advanced Turbulence Models," *AIAA Journal*, Vol. 26, No. 11, 1988, pp. 1299–1310.

[30]Barakos, G., and Drikakis, D., "NACA0012 Airfoil, 2D Steady and Unsteady Flow," *Progress in Computational Flow–Structure Interaction*, edited by W. Haase, V. Selmin, and B. Winzell, Notes on Numerical Fluid Mechanics and Multidisciplinary Design, Vol. 81, Springer, Berlin, 2003, Chap. 4.1.

[31]Schreck, S. J., Addington, G. A., and Luttges, M. W., "Flow Field Structure and Development Near the Root of a Straight Wing Pitching at Constant Rate," AIAA Paper 91-1793, Sept. 1991.